Biomaterials Science

ROYAL SOCIETY OF CHEMISTRY

PAPER

View Article Online
View Journal | View Issue

Cite this: *Biomater. Sci.*, 2023, **11**, 5931

Co-delivery of vitamin D3 and Lkb1 siRNA by cationic lipid-assisted PEG-PLGA nanoparticles to effectively remodel the immune system *in vivo*†

Haochuan Liu, [a,c] Yuning Zhang,[a,b,e] He Li,[a,e] Xue Gao,[a] Jialiang Wang,[a,e] Xiuxiu Cong,[a,e] Yanbao Xin,[a,e] Qingsan Zhu, [c] Bing Chen,*[d] Yong-Guang Yang[a,b,e] and Tianmeng Sun *[a,b,e,f]

Received 4th May 2023,
Accepted 4th July 2023

DOI: 10.1039/d3bm00767g

rsc.li/biomaterials-science

The imbalance of the immune system can lead to the occurrence of autoimmune diseases. Controlling and regulating the proliferation and function of effector T (Teff) cells and regulatory T (Treg) cells becomes the key to treating these diseases. Dendritic cells (DCs), as dedicated antigen-presenting cells, play a key role in inducing the differentiation of naive CD4+ T cells. In this study, we designed a cationic lipid-assisted PEG-PLGA nanoparticle (NPs/VD3/siLkb1) to deliver 1,25-dihydroxyvitamin D3 (VD3) and small interfering RNA (siRNA) to DC cells in the draining lymph nodes. By modulating the phenotypic changes of DC cells, this approach expands Treg cells and reduces the occurrence of autoimmune diseases. Thus, this study provides a novel approach to alleviating the occurrence and development of autoimmune diseases while also minimizing the risk of unwanted complications.

Introduction

Multiple sclerosis (MS) is a chronic autoimmune disease with inflammatory demyelination of the central nervous system as the main pathological change, which lacks effective treatment in clinic. Autoimmune diseases are due to an imbalance of the immune system caused by the body's misidentification of autoantigens. The experimental autoimmune encephalomyelitis (EAE) model was first established in 1935,[1] and it is a classic animal model for studying multiple sclerosis. Because of its clinical manifestations, histopathological and immunologic changes are similar to those of multiple sclerosis.

Dendritic cells constitute the most potent group of dedicated antigen-presenting cells within the body, involved in both innate and adaptive immune responses. They serve dual functions in immune response and immune tolerance, contributing significantly to the maintenance of immune balance in autoimmune diseases.[2] Tolerant dendritic cells (TolDCs), stable and semi-mature subpopulations intermediate between antigen-captured immature DCs (iDCs) and immunogenic mature DCs (mDCs), promote immune tolerance. TolDCs regulate peripheral tolerance against autoantigens by exhibiting low expression of co-stimulatory molecules, secreting anti-inflammatory cytokines, and inducing effector T cell weakness as well as regulatory T cell proliferation.[3,4]

T-Helper type 1 (Th1) and T-helper type 17 (Th17) cells, subsets of pathogenic T cells, play significant roles in the pathogenesis of autoimmune diseases.[5] Dendritic cells (DCs) are instrumental in the activation of both Th1 and Th17 cells. In the peripheral lymphoid organs of animal models with experimental autoimmune encephalomyelitis (EAE), DCs bind to T cells through surface molecules, providing costimulatory signals that promote the polarization of Th1 and Th17 cells. Consequently, these T cells are activated by dendritic cells and other antigen-presenting cells, cross the blood–brain barrier, and are involved in mediating the demyelination of the central nervous system.[6] Regulatory T cells (Treg cells), a group of lymphocytes, negatively regulate the body's immune response, maintaining peripheral immune tolerance and preventing

[a]*Key Laboratory of Organ Regeneration and Transplantation of Ministry of Education, Jilin University, Changchun, Jilin, 130061, China. E-mail: tsun41@jlu.edu.cn*
[b]*International Center of Future Science, Jilin University, Changchun, Jilin, 130015, China*
[c]*Department of Orthopaedics, China-Japan Union Hospital of Jilin University, Changchun, Jilin, 130031, China*
[d]*Department of Anesthesiology, China-Japan Union Hospital of Jilin University, Changchun, Jilin, 130031, China. E-mail: chenbing2020@jlu.edu.cn*
[e]*National-local Joint Engineering Laboratory of Animal Models for Human Diseases, Changchun, Jilin, 130062, China*
[f]*State Key Laboratory of Supramolecular Structure and Materials, Jilin University, Changchun, Jilin, 130012, China*
† Electronic supplementary information (ESI) available. See DOI: https://doi.org/10.1039/d3bm00767g

excessive immune response and damage to the body. Produced by the thymus and exported to the periphery, Treg cells reduce the activation and proliferation of potential autoreactive T cells present in the normal body by secreting cytokines or through direct contact, thus preventing the occurrence of autoimmune diseases.[7]

Given the therapeutic effect of Treg in autoimmune diseases, enhancing their proliferation and function can be applied in the treatment of such conditions. 1,25-Hydroxyvitamin D3, an activated form of vitamin D, participates in the immunomodulatory process of the body, primarily relying on the vitamin D receptor (VDR), which is expressed on all immune cells.[8,9] VD3 facilitates the differentiation of DCs into TolDCs, stimulating Treg amplification,[10] the secretion of anti-inflammatory cytokines IL-10,[11] and the reduction of inflammatory Th17 lymphocytes[12] and pro-inflammatory cytokines IL-17.[13] However, long-term administration of VD3, even in small doses, may lead to toxic side effects such as hypercalcemia.[14] Consequently, to attenuate the therapeutic dose of VD3, alleviate side effects, and expand the Treg pool, our research group incorporated liver kinase B1 (Lkb1) in the study.

Lkb1, a central regulator of cellular metabolism and growth, has been found to cause lipid accumulation and glycolysis upregulation in peripheral DCs when deficient, leading to metabolic disorders and enhanced immunogenicity. Interestingly, this phenotype with enhanced maturation capacity also enables DCs to increase the development and expansion of thymic Treg under homeostatic conditions, ultimately leading to immunosuppressive effects,[15] as demonstrated by a reduced ability to control tumor growth and protect against allergic asthma.[16] This evidence suggests that Lkb1 acts as an important rheostat in DCs to maintain immune homeostasis by regulating the balance between proinflammatory and regulatory T cell responses. Our group used siRNA as an RNA interference technique (RNAi) to reduce Lkb1 expression. Although siRNA has been highly effective in gene silencing, suitable delivery vehicles are still required to transport it to the target site due to nuclease hydrolysis, cell membrane charge repulsion, various biological barriers, and off-target effects.[17–20]

The drug delivery system based on engineering precision nanoparticles has become a research hotspot, improving drug solubility and distribution.[21] Engineered precision nanoparticles are diverse, with developed drug delivery systems, including polymeric NPs, lipid-based NPs, and inorganic NPs. Biodegradable polymer nanoparticles can serve as a versatile platform for signaling to the immune system, offering variable drug delivery capabilities. Therapeutics can be encapsulated within the NP core, wrapped in the polymer matrix, chemically conjugated to the polymer, or bound to the NP surface. This enables delivery of multidrug compounds, including hydrophobic and hydrophilic substances, as well as cargos with different molecular weights.[22–25] Simultaneously, surface modification can be easily performed for additional targeting, and the nanoparticles are designed to precisely control the encapsulation effect and release kinetics of encapsulated drugs, thereby improving drug solubility and prolonging drug half-life. It also reduces toxic side effects and synergistically facilitates drug penetration through biological barriers.[21]

In this study, we report the co-delivery of VD3 and Lkb1-siRNA into DCs using a cationic lipid-assisted PEG-PLGA nanoparticles to modulate phenotypic changes, maintain immune tolerance, and inhibit the development of EAE disease models by expanding Tregs. This study provides new insights for treating autoimmune diseases and regulating the immune microenvironment.

Materials and methods

Chemicals, antibodies, and cells

Poly(ethylene glycol)-poly(D,L-lactic-*co*-glycolide) ($PEG_{5\ K}$-$PLGA_{10\ K}$) was purchased from Kelan Bio Co. (Guangzhou, China), while 1,2-dioleoyl-3-trimethylammonium-propane (DOTAP) was acquired from Corden Pharma (Liestal, Switzerland). Additionally, 1α,25-dihydroxyvitaminD3 (VD3) was purchased from J&K Scientific Co. (Beijing, China), and Myelin oligodendrocyte glycoprotein 35–55 (MOG35–55) peptide was purchased from Genscript Biotech Co. (Nanjing, China). Roswell Park Memorial Institute (RPMI) 1640, phosphate-buffered saline (PBS), penicillin/streptomycin, L-glutamine, fetal bovine serum (FBS), trypan blue and 0.25% trypsin were all sourced from Life Technologies (Gibco, CA, USA). Moreover, the Aqua dead cell stain kit was obtained from Invitrogen (Carlsbad, CA, USA), and the red blood cell lysis buffer was purchased from Solarbio (Beijing, China). 1,1′-Dioctadecyl-3,3,3′,3′-tetramethylindocarbocyanine perchlorate (DiI) was purchased from Sigma-Aldrich (Saint Louis, MS, USA).

Fluorescence-labeled rat anti-mouse CD11b, CD11c, I-A/I-E, CD80, CD86, CD40, CD45, CD3, CD4, CD25, Foxp3, CD8, and CD19 monoclonal antibodies were obtained from Biolegend (San Diego, CA, USA) and BD Biosciences (Franklin Lakes, NJ, USA). Mouse granulocyte-macrophage colony-stimulating factor (GM-CSF) was purchased from R&D (Minneapolis, MN, USA), and Mouse IL-4 was purchased from Peprotech (Rocky Hill, NJ, USA). siRNA targeting Lkb1-mus-625 (Lkb1-siRNA, antisense strand, 5′-AUUGGUGGUGAGUAGCAGGTT-3′), negative control siRNA with a scrambled sequence (NC-siRNA, antisense strand, 5′-ACGUGACACGUUCGGAGAATT-3′), and fluorescently labeled Cy5-siRNA were synthesized by Suzhou Ribo Life Science Co. (Kunshan, China).

The dendritic cell line DC1.2 was purchased from the American Type Culture Collection (ATCC). DC1.2 cells were cultured in RPMI1640 supplemented with 10% FBS at 37 °C in an incubator with 5% CO2. Bone marrow (BM) cells were flushed out of the femurs and tibias of C57NL/6 mice. Bone marrow-derived DCs (BMDCs) were generated by culturing cells for 7d in culture medium containing 10 ng mL^{-1} mouse IL-4 and GM-CSF. The medium was changed every two days until the cells were harvested for *in vitro* analysis.

Animal

Female C57/B6J mice, aged 6–8 weeks, were collected from Charles River (Beijing, China) and housed in a specific patho-

gen-free environment with *ad libitum* access to food and water. All animals were maintained in accordance with the Guidelines for The Care and Use of Laboratory Animals. The experimental procedures were approved by the Jilin University Animal Care and Use Committee.

Preparation of nanocomposites

In the preparation of our dual-agent nanocomposites, the water-in-oil-in-water double emulsion solvent evaporation method was deemed suitable. The inner aqueous phase consisted of siRNA (0.2 mg) in 25 μL of RNase-free water, while the organic phase contained 500 μl of chloroform with 25 mg of encapsulating polymer, 3 mg of cationic lipid material, and 10 ng of VD3. The first emulsification was performed using a sonicator (VCX130, Sonics & Materials, Inc. Newtown, CT, USA) at 60% *amplitude* and ice bath ultrasonication for 60 seconds (pausing 1 s every 4 s). Subsequently, 5 ml of ultra-pure water was introduced to the water-in-oil emulsion. The water-in-oil-in-water emulsion was generated by 60% amplitude ultrasonic action for 60 s (pausing 1 s every 10 s) in an ice bath. Rotary evaporator (R-210, Buchi, Switzerland) removed chloroform, and the supernatant was collected for encapsulation efficiency analyses. Nanoparticles were centrifuged at 30 000*g* using a high-speed microcentrifuge (Beckman, USA) for 30 min, rinsed twice with sterile water, and subsequently re-dispersed in ultra-pure water. For fluorescent dye (DiI)-labeled NPs, the dye was incorporated into chloroform at a 0.1% mass ratio during synthesis. PEG-PLGA nanoparticle size and zeta potential were monitored by Zetasizer NanoZS90 (Malvern Instruments, Southborough, UK) at 25 °C.

Loading efficiency and *in vitro* release

VD3 quantitative analysis was conducted using high-performance liquid chromatography (HPLC, Youngling YL 9100 HPLC system, South Korea). The detection wavelength for VD3 was 265 nm, and the column employed for separation was Zorbax SB-C18 (3 × 150 mm, 3.5 μm particle size). The column temperature was kept at 25 °C, the total flow rate was 0.5 ml min^{-1}, the sample volume was 20 μl, and each sample's run time was 13 min. A mobile phase consisting of acetonitrile/water (90 : 8 : 2, v/v) was applied. The calibration curve was established from samples with various concentrations (3.90625–4000 ng mL^{-1}). Following the HPLC analysis method validation for precise VD3 quantification, the VD3 amount loaded into the particles was determined using the calibration curve. The VD3 encapsulation efficiency (EE) in the PVD3s was calculated according to the equation:

$$\text{EE}\,(\%) = \text{loaded VD3 amount in particle/feed VD3 amount} \times 100$$

NPs/VD3 and NPs/VD3/siLkb1 particles loaded with 500 ng of VD3 were suspended in 500 μL of ultra-pure water and transferred to dialysis tubes (3.5 kDa, Spectrum, USA). The tubes were then immersed in 15 mL PBS and maintained at 37 °C in a 100 strokes per min water bath. External buffers were collected at predetermined intervals, and the VD3 release concentration was determined by high-performance liquid chromatography (HPLC).

In vitro Lkb1 gene silencing with NPs/siLkb1

DC1.2 cells were seeded in 24-well plates at a density of 5×10^4 cells per well and incubated at 37 °C overnight. Following this, cells were transfected with NPs/siLkb1 and other controls in 10% RPMI 1640 (pH 7.4 or 6.8) at an siRNA dose of 100 nM. Blank-NPs and Lipofectamine 2000-transfected Lkb1-siRNAs served as negative and positive controls, respectively. After 6 hours of incubation, the medium in each well was replaced with complete 10% RPMI 1640. Cells were harvested 24 hours post-transfection, and Lkb1 expression was determined through quantitative real-time PCR.

Total RNA from NPs/siLkb1 and control transfected cells was extracted using Trizol. cDNA was synthesized with HiScript II Q RT SuperMix for qPCR (+gDNA wiper) (Vazyme, Nanjing, China). To measure Lkb1 mRNA expression levels, cDNA underwent qPCR analysis targeting Lkb1 and β-actin using the ChamQ Universal SYBR qPCR Master Mix (Vazyme, Nanjing, China). The StepOnePlus Real-Time PCR system (Applied Biosystems) executed the quantitative real-time PCR, and cycle threshold (Ct) values were calculated using StepOne Software (Applied Biosystems). Primers for mouse Lkb1 and β-actin were as follows:

Lkb1, 5′-GGACGTGCTGTACAATGAGG-3′ (forward) and 5′-GCATGCCACATACGCAGT-3′ (reverse);

β-Actin, 5′-ATATCGCTGCGCTGGTCGTC-3′ (forward) and 5′-AGGATGGCGTGAGGGAGAGC-3′ (reverse).

Cellular uptake of nanoparticles

DC1.2 cells (5×10^4) were seeded into 24-well plates and cultured for 24 hours to reach 50% confluency. Subsequently, cells were incubated at 37 °C for 2 hours with NPs/DiI/Cy5-siNC suspended in complete RPMI1640 medium at an siRNA concentration of 200 nM. PBS, NPs/DiI, and NPs/Cy5-siNC were used as controls.

For fluorescence microscopy observation, DC1.2 cells were fixed with acetone for 30 min at −20 °C and stained with Phalloidin-AF488 for cytoskeleton visualization. Coverslips were mounted on glass microscope slides, nuclei were stained with a drop of antifade mounting medium containing DAPI, and photobleaching was reduced. Cellular uptake of nanoparticles was visualized using a laser scanning confocal microscope (Carl Zeiss, Oberkochen, Germany).

For flow cytometry analysis, DC1.2 cells were trypsinized and washed with PBS. Cells from each sample were stained with appropriate dilutions of various combinations. Stained cells were analyzed using a LSRII Flow Cytometer with BD FACSDiva software (BD Bioscience), and data were processed using Flowjo software.

Biodistribution of NPs *in vivo*

Twenty-four hours after intradermal injection of NPs/DiI/Cy5-siNC and PBS into the inguinal region in C57BL/6J mice, the

distribution of nanoparticles was performed using an IVIS Spectrum *In Vivo* Imaging system (PerkinElmer, USA). Mice were sacrificed 24 hours post-injection, and various tissues, including the brain, heart, lung, liver, spleen, kidney, and draining lymph node, were harvested and imaged with the IVIS Spectrum In Vivo Imaging system. Data analysis was conducted using Living Image software (Caliper Life Sciences).

Confocal laser scanning microscopy imaging

Bilateral draining lymph nodes were harvested from C57BL/6J mice 24 hours after the injection of NP/DiI/Cy5-siNC or PBS into unilateral draining lymph nodes. Lymph nodes were fixed in 4% paraformaldehyde overnight, then immersed in a 30% sucrose solution overnight. Subsequently, lymph nodes were sectioned into 5 μm slices and stained with DAPI and CD11c-AF488 according to the provided protocol. Images were captured using a Zeiss LSM 880 confocal laser scanning microscope with a 40× objective (Carl Zeiss, Oberkochen, Germany).

NPs affect BMDC differentiation *in vitro*

BMDCs were generated by flushing BM cells from the tibia and femur of C57BL/6 mice and culturing them for seven days in RPMI 1640 medium supplemented with 10% FBS, mouse IL-4 (10 ng ml^{-1}), and GM-CSF. Following a 24-hour incubation with PBS, free-VD3, NPs/siNC, NPs/VD3, NPs/siLkb1, and NPs/VD3/siLkb1, the cells were further stimulated with ovalbumin (OVA, 10 μg mL^{-1}) for an additional 24 hours. Cells were then harvested and washed twice with PBS. The expression of CD80, CD86, CD40, and MHC-II (I-A/I-E) on BMDCs ($CD11b^{+}CD11c^{+}$) was determined by flow cytometry.

Induction of EAE, assessment of clinical signs, and administration route

C57/B6J mice (18–20 g) were subcutaneously injected with myelin oligodendrocyte glycoprotein (MOG) $_{35–55}$ polypeptide (Genscript, Nanjing, China) emulsified with complete Freund's adjuvant (CFA, Sigma-Aldrich, Missouri, USA) containing 8 mg ml^{-1} thermally inactivated *Mycobacterium tuberculosis* (Difco, Michigan, USA). Mice were then intraperitoneally injected with 300 ng of pertussis toxin (PTX, Calbiochem, USA) at 0 and 48 hours post-immunization. EAE clinical scores were graded according to the criteria proposed by Kono *et al.*:[26] 0, asymptomatic; 1, tail paralysis or shambling; 2, severe single hind limb paralysis or mild double hind limb paralysis; 3, severe paralysis of both hind limbs; 4, severe paralysis of both hind limbs with forelimbs involved; 5, moribund or dead. Nanoparticles were administered intradermally through bilateral inguinal draining lymph nodes once before induction and 4 times after induction (every other day).

Histopathology

On day 20 post-immunization, spinal cords were harvested from all rats, fixed, paraffin-embedded, sectioned at 5 μm thickness, and subsequently stained with hematoxylin and eosin (H&E) for histopathological examination. Demyelination was detected by Luxol fast blue (LFB) staining.

Flow cytometry analysis

Twenty-four hours after administering the last dose, C57/B6J mice were sacrificed, and bilateral inguinal draining lymph nodes, blood, and spleen were harvested. Lymph node and spleen cells were isolated by grinding the spleens through 40 μm filters, followed by centrifugation at 1650 rpm for 5 minutes. The resultant pellet was re-suspended in FACS buffer and sequentially filtered through 40 μm mesh filters to remove debris and cellular fragments. After lysing red blood cells, blood cells and splenic cells were washed and resuspended in FACS buffer. The cells were then stained with appropriate dilutions of various combinations of the following fluorescence-labeled antibodies: anti-CD11b, anti-CD11c, anti I-A/I-E, anti-CD86, anti-CD80, anti-CD40, anti-CD45, anti-CD3, anti-CD4, anti-CD25, anti-Foxp3, anti-CD8, and anti-CD19. Stained cells were acquired on an LSRII Flow Cytometer using BD FACS Diva software (BD Bioscience), and data were analyzed using Flowjo software.

Statistical analysis

The data were represented as the mean ± standard error. Differences were analyzed using one-way analysis of variance (ANOVA) and the Student's *t*-test. Results with a $p < 0.05$ were considered statistically significant.

Results

Preparation and characterization of PEG-PLGA nanoparticles co-loaded with VD3 and siLkb1

In this study, PEG-PLGA nanoparticles were prepared using the double emulsion method (Fig. 1A). The resulting particles' size (Fig. 1B) and surface potential (Fig. 1C) were characterized using a dynamic light scattering (DLS) particle size analyzer. The particle sizes of NPs/siNC, NPs/VD3, NPs/siLkb1, and NPs/VD3/siLkb1 were 97.9 ± 0.5 nm, 86.3 ± 0.7 nm, 107.1 ± 0.2 nm, and 108.1 ± 0.5 nm, respectively, while the surface potentials were 38.8 ± 1.67 mV, 22.3 ± 0.35 mV, 36.9 ± 1.85 mV, 22.3 ± 0.35 mV, and 34 ± 1.51 mV. The entrapment efficiencies of VD3 in NPs/VD3 and NPs/VD3/siLkb1 were approximately 7% and 16%, respectively. Moreover, the encapsulation efficiency of siRNA by particles exceeded 90%, as determined by gel retardation (Fig. 1D). The *in vitro* drug release of VD3-loaded nanoparticles was further evaluated, revealing that nearly 79.8% of VD3 was released after 48 hours of incubation in PBS when encapsulated in nanoparticles, compared to free-VD3 (Fig. 1E). This finding demonstrates that NPs encapsulation could extend the release time of VD3, thereby prolonging the drug's circulatory half-life. The efficacy of NPs/siLkb1 in inhibiting Lkb1 expression *in vitro* was measured using real-time PCR (RT-PCR) (Fig. 1F). Results indicated that DC1.2 cells incubated with NPs/siLkb1 showed a significant decrease in Lkb1 mRNA levels compared to those treated with NPs/Blank, suggesting that NPs/siLkb1 can effectively downregulate Lkb1 expression in DC1.2 *in vitro*.

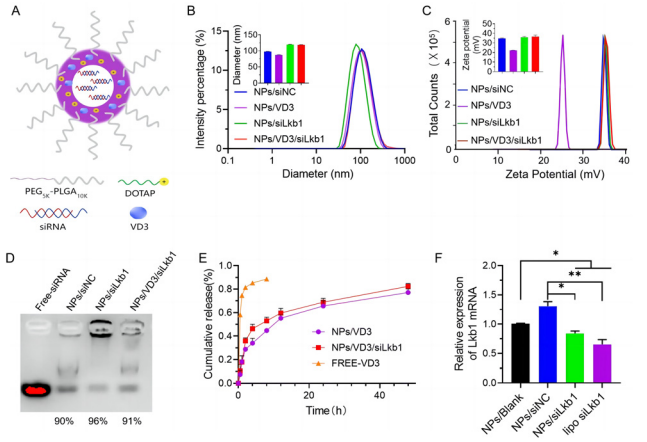

Fig. 1 The characterization of nanoparticles. (A) Schematic illustration of the synthesis of polymer nanoparticles *via* the double emulsification method. (B) Particle sizes for NPs/siNC, NPs/VD3, NPs/siLkb1, and NPs/VD3/siLkb1. (C) The zeta potential of NPs/siNC, NPs/VD3, NPs/siLkb1, and NPs/VD3/siLkb1. (D) Gel retardation assay of siRNA and NPs. (E) The cumulative release of VD3 from free-VD3, NPs/VD3, and NPs/VD3/siLkb1 incubated in PBS. (F) The relative mRNA levels of DC1.2 upon treatment with NPs/siLkb1 for 24 h were assayed by quantitative real-time PCR. Statistical significance is denoted with an asterisk (*): $P < 0.05$; double asterisks (**): $P < 0.01$. Data are presented as mean ± S.E.M. (n = 3).

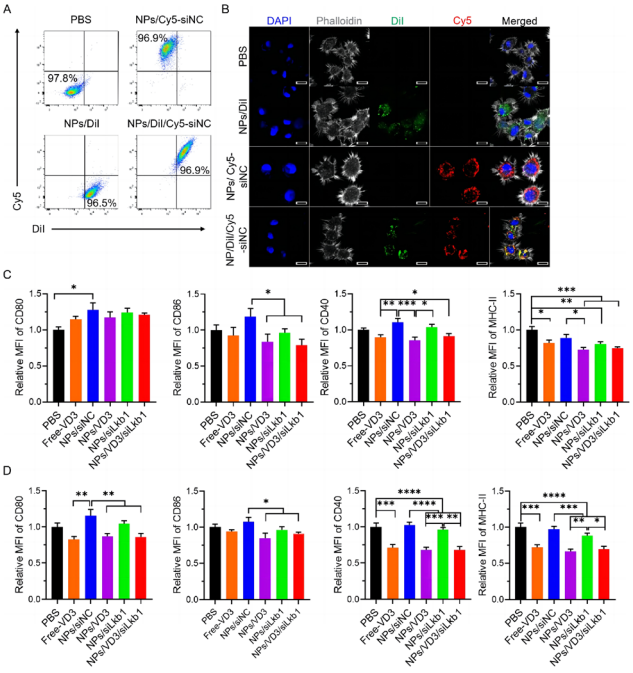

Fig. 2 NPs/VD3/siLkb1 maintain a tolerant phenotype *in vitro* for DC cells. (A) Representative flow cytometric images of DC1.2 cells demonstrating cellular uptake of NPs/DiI, NPs/Cy5-siNC, or NP/DiI/Cy5-siNC. (B) Confocal laser scanning microscope (CLSM) images of DC1.2 cells after a 2-hour incubation with PBS, NPs/DiI, NPs/Cy5-siNC, or NP/DiI/Cy5-siNC. DiI and Cy5 fluorescence signals were pseudo-stained green and red, respectively, with cell membranes and nuclei stained using Phalloidin-AF488 (white) and DAPI (blue). The scale bar measures 20 μm. (C and D) NPs containing different drugs significantly affect the expression of DC surface molecules *in vitro*. BMDC were co-cultured with PBS, Free-VD3, NPs/siNC, NPs/VD3, NPs/siLkb1, and NPs/VD3/siLkb1 for 24 hours, followed by a 24-hour stimulation with OVA (D) or no stimulation (C). Expression of CD80, CD86, CD40, and MHC-II detected by flow cytometry. Statistical significance is denoted with an asterisk (*): $P < 0.05$; double asterisks (**): $P < 0.01$. Data are presented as mean ± S.E.M.

NPs/VD3/siLkb1 significantly promote the generation of tolerogenic DCs *in vitro*

Before examining the impact of NPs/VD3/siLkb1 on the phenotype of DC cells, we assessed the capacity of PEG-PLGA nanoparticles to concurrently deliver both hydrophilic and hydrophobic drugs to the same cells. We chose the hydrophobic fluorescent material DiI and hydrophilic Cy5-siNC as model preparations for nanoparticles (NPs/DiI/Cy5-siNC), and evaluated their distribution in DC cells by detecting the intracellular fluorescence signals of DiI and Cy5 using a flow cytometer. In contrast to PBS, nearly all DC1.2 cells treated with NPs/DiI/Cy5-siNC were DiI and Cy5 double-positive cells, whereas NPs/DiI- or NPs/Cy5-siNC-treated cells were DiI or Cy5 single-positive cells (Fig. 2A). The intracellular distribution of NPs/DiI/Cy5-siNC in DC1.2 cells was further observed through confocal laser scanning microscopy (CLSM). After incubation with NPs/DiI/Cy5-siNC, the fluorescence signal of DiI and Cy5 exhibited a partially overlapping distribution in the cytoplasm of DC1.2 cells, with DiI or Cy5 signals also clearly detected in the cytoplasm of cells treated with NPs/DiI or NPs/Cy5-siNC, respectively (Fig. 2B).

Subsequently, we incubated BMDC from C57/B6J mice with drug-loaded nanoparticles and controls for eight days and identified the phenotype. The results showed that Free-VD3, NPs/VD3, and NPs/VD3/siLkb1 downregulated the expression of CD86, CD40, and MHC-II on DCs, while the expression of CD80 did not significantly decrease (Fig. 2C). Nevertheless, after BMDC stimulation with OVA, Free-VD3, NPs/VD3, and NPs/VD3/siLkb1 maintained low expression of CD86, CD40, and MHC-II, and CD80 expression was also lower than that of the control groups (Fig. 2D). Additionally, the surface antigen expression of the NPs/siLkb1 treatment group decreased compared to NPs/siNC, but without statistical difference.

Based on these findings, we can conclude that PEG-PLGA nanoparticles can be effectively phagocytosed by DC cells *in vitro*, simultaneously releasing drugs in DCs. Furthermore, NPs/VD3/siLkb1 can effectively induce the differentiation of DCs to the TolDC phenotype *in vitro* and maintain their tolerant phenotype after stimulation with sensitizing antigens.

NPs/VD3/siLkb1 effectively accumulate in lymph nodes and deliver both VD3 and siLkb1 into DCs *in vivo*

To determine the localization of nanoparticles in draining lymph nodes of DC cells *in vivo*, we administered NPs/DiI/Cy5-siNC *via* intradermal injection into the unilateral inguinal region of mice and subsequently examined the fluorescence biodistribution. Twenty-four hours post-injection, fluorescence

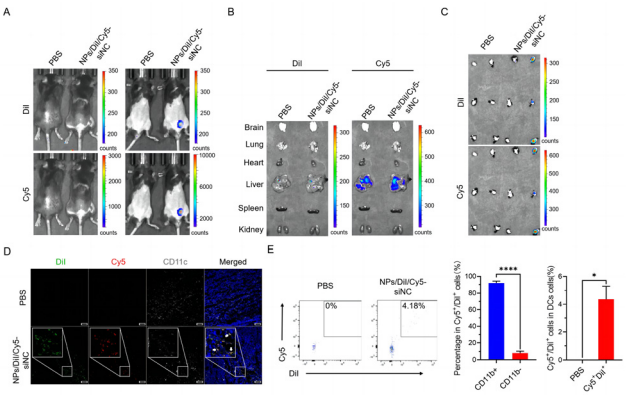

Fig. 3 The biodistribution of drug-loaded nanoparticles in mice. (A) *In vivo* fluorescence images were obtained 24 hours after intradermal injection of PBS or NPs/DiI/Cy5-siNC into the unilateral inguinal region of C57BL/6 mice. (B and C) Representative *ex vivo* fluorescent images of excised organs (brain, lung, heart, liver, spleen, kidney (B), and draining lymph node (C)) at 24 hours post-administration of PBS or NPs/DiI/Cy5-siNC. (D) CLSM images depicting the distribution of Cy5-siRNA and DiI in draining lymph nodes 24 hours after intradermal injection of PBS or NPs/DiI/Cy5-siNC. Nuclei were stained with DAPI (blue), CD11c + with AF488 (white), and NPs were labeled with DiI (green) and Cy5 (red). The scale bar measures 20 μm. (E) Representative flow cytometry plots of lymph nodes from C57BL/6 mice and the frequency of Cy5+/DiI+ in dendritic cells are shown. Statistical significance is denoted with an asterisk (*): $P < 0.05$; double asterisks (**): $P < 0.01$. Data are presented as mean ± S.E.M.

signals of DiI and Cy5 in the inguinal area were detected in the NPs/DiI/Cy5-siNC group compared to PBS (Fig. 3A). Furthermore, the enrichment of DiI and Cy5 fluorescence signals was observed in the draining lymph nodes of isolated mouse organs in the NPs/DiI/Cy5-siNC treated group (Fig. 3B and C). Confocal laser scanning microscopy (CLSM) images of draining lymph node sections showed an accumulation of drug-loaded nanoparticles within the lymph nodes. DiI and Cy5 fluorescence signals co-localized, with the majority of signals located in $CD11c^+$ cells. In contrast, no DiI and Cy5 fluorescence signals were detected in the lymph nodes of PBS-treated mice (Fig. 3D). Flow cytometry analysis yielded similar results, revealing that more than 85% of DiI and Cy5 double-positive fluorescence signals were enriched in $CD11b^+$ cells in the lymph nodes of mice treated with NPs/DiI/Cy5-siNC. Additionally, DCs in the lymph nodes of NPs/DiI/Cy5-siNC-treated mice exhibited significantly higher fluorescence signal enrichment compared to PBS-treated mice (Fig. 3E). These findings indicate that both hydrophilic and hydrophobic drugs encapsulated in PEG-PLGA nanoparticles can be effectively delivered to the lymph nodes and phagocytosed by DC cells.

NPs/VD3/siLkb1 significantly promote the generation of tolerogenic DCs and increase the Treg amount *in vivo*

Upon confirming that DCs in the draining lymph nodes can phagocytose nanoparticles, we administered the drug-loaded nanoparticles NPs/VD3/siLkb1, NPs/VD3, NPs/siLkb1, and control groups PBS and NPs/siNC into mice *via* intradermal injection in the groin. Subsequently, the mice were sacrificed 24- and 48-hours post-injection to obtain draining lymph nodes, spleen, and peripheral blood samples. Flow cytometry analysis revealed that NPs/VD3/siLkb1 significantly down-regulated CD40 and MHC-II expression on DCs and reduced the proportion of DC cells in the draining lymph nodes of mice (Fig. 4A, and S2B†). However, CD86 expression showed a downward trend without statistical difference compared to other groups, and CD80 expression remained unchanged. NPs/VD3 was more effective in reducing CD40 expression than NPs/VD3/siLkb1, but the latter demonstrated a more pronounced effect in decreasing MHC-II expression levels (Fig. 4A).

We evaluated the proportion and count of Treg cells in the lymph nodes, spleen, and peripheral blood. In the lymph nodes (Fig. 4B, E, and S2D†) and spleen (Fig. 4C, and S2E†) of mice treated with NPs/VD3/siLkb1 for 24 hours, the Treg cell ratios in $CD45^+$ cells, $CD4^+$ T cells, and Treg/$CD8^+$T cells all increased. The Treg count in lymph nodes was significantly higher than that in PBS and NPs/siNC. In the spleen, the Treg count was significantly higher compared to NPs/siNC, but showed no statistical difference when compared to PBS. The proportion and count of Treg cells in NPs/VD3 and NPs/siLkb1 were slightly higher than those in NPs/siNC, lower than those in the NPs/VD3/siLkb1 group, but without statistical difference. No significant difference was observed in the proportion and count of Treg cells treated with NPs/VD3 and NPs/siLkb1 in lymph nodes compared to PBS, with a slight decrease

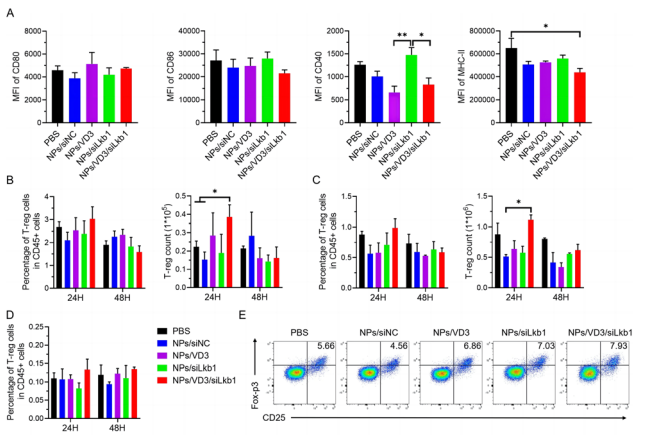

Fig. 4 Impact on immune cells of drug-loaded nanoparticles in mice. (A) Effects of NPs containing different drugs on the expression of dendritic cell surface molecules *in vivo*. Following intradermal injection in the inguinal region for 48 hours, the expression of CD80, CD86, CD40, and MHC-II in DC cells obtained from lymph nodes was analyzed by flow cytometry. (B–D) Alterations in Treg levels in peripheral immune organs. After intradermal injection in the inguinal region, NPs/VD3/siLkb1 increased Treg levels and counts in lymph nodes (B) and the spleen (C) at 24 h post-injection, subsequently decreasing after 48 h. Treg levels in peripheral blood (D) remained comparable to the 24 h levels at 48 h. (E) Representative flow cytometry of Tregs in lymph nodes of C57BL/6 mice 24 hours after intradermal injection. Statistical significance is denoted with an asterisk (*): $P < 0.05$; double asterisks (**): $P < 0.01$. Data are presented as mean ± S.E.M.

observed in the spleen, but no statistical difference. At 48 hours post-administration, the proportion and quantity of Treg decreased in each drug-loaded nanoparticle treatment group. In peripheral blood, the proportion of Treg at 48 h was similar to the 24 h levels in each group (Fig. 4D).

Based on the above-mentioned findings, NPs/VD3/siLkb1 can induce DC differentiation to the tolDC phenotype *in vivo* while amplifying Treg in the draining lymph nodes and spleen to a certain extent within 24 hours. Although NPs/siLkb1 could not induce a tolDC phenotype, the Treg pool in lymph nodes and the spleen was slightly higher than NPs/siNC within 24 hours. However, at 48 hours post-injection, Treg levels in the draining lymph nodes and spleen decreased, while Treg amounts in the peripheral blood remained constant.

NPs/VD3/siLkb1 effectively delay the onset and inhibit the development of EAE

To assess the impact of NPs/VD3/siLkb1 on EAE pathogenesis, NPs/VD3/siLkb1 and other groups were intradermally injected into EAE mice *via* the inguinal area one day before immune response induction, and on days 1, 3, 5, and 7 following immunization (Fig. 5A). As demonstrated by the mice's weight changes, weight loss was positively correlated with disease severity. Notably, even a small dose of VD3 induced weight loss in mice (Fig. S3†). All nanoparticle administration groups exhibited some inhibitory effects on EAE pathogenesis; however, compared to other groups, EAE mice receiving NPs/VD3/siLkb1 displayed a lower onset time and clinical score at the peak of onset (mean clinical score in each group: PBS, 2.9 ± 0.995; NPs/siNC, 2.3 ± 1.16; NPs/VD3, 2.1 ± 1.45; NPs/siLkb 1, 2.3 ± 0.95; NPs/VD3/siLkb1, 1.9 ± 1.36). However, during the recovery period, clinical scores for each group converged at similar levels (Fig. 5B). Histological evaluation, conducted through H&E and LFB staining, revealed results consistent with clinical scores. The NPs/VD3/siLkb1-treated group exhibited significantly enhanced protection against spinal cord inflammatory cell infiltration and white matter demyelination compared to both the NPs/VD3- and NPs/siLkb1-treated groups, whereas the PBS- and NPs/siNC-treated groups demonstrated the most severe effects (Fig. 5C).

Flow cytometry analysis indicated that the proportion of DCs in the draining lymph nodes of NPs/VD3/siLkb1-treated EAE mice was significantly decreased, and the expression of CD86, CD40, and MHC-II on DC cells was significantly lower than in other groups, while CD80 expression remained statistically unchanged (Fig. 5D). These findings corroborate previous *in vitro* and *in vivo* results, suggesting that NPs/VD3/siLkb1 can direct DCs toward a tolerogenic phenotype in the lymph nodes of EAE mice.

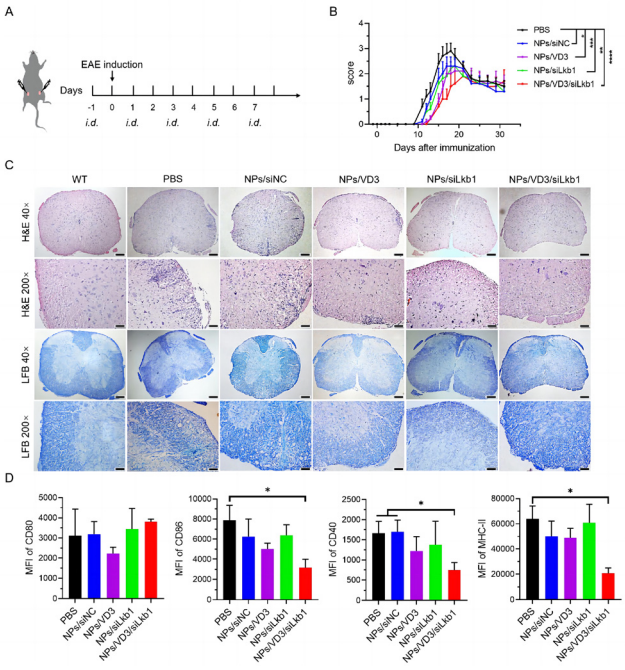

Fig. 5 NPs/VD3/siLkb1 inhibits EAE pathogenesis. (A) Schematic representation of EAE mice treated with NPs/VD3/siLkb1 and other controls. C57BL/6 mice received intradermal injections of PBS, NPs/siNC, NPs/VD3, NPs/siLkb1, or NPs/VD3/siLkb1 every other day for a total of 5 times (VD3 dose: 10 ng per mouse; Lkb1-siRNA dose: 3.5 μg per mouse) starting from one day before the EAE ; the EAE mice model was induced on day 0 (n = 10 per group). (B) EAE clinical scores were measured every other day. EAE mice treated with NPs/VD3/siLkb1 exhibited a delayed onset time and a reduced clinical score at peak onset. (C) EAE mice received NPs loaded with different drugs and were sacrificed when the PBS group reached peak disease severity (day 20). Lumbar enlargement and spinal cord tissue were excised and fixed with 4% paraformaldehyde. Histological evaluation of NPs/VD3/siLkb1-treated mice revealed reduced inflammatory cell infiltration in H&E staining and less white matter demyelination and structural damage in LFB staining compared to other groups. (D) Mice were sacrificed 24 hours after the final administration, and bilateral draining lymph nodes were collected. The expression of CD80, CD86, CD40, and MHC-II in DC cells obtained from lymph nodes was detected by flow cytometry. Statistical significance is denoted with an asterisk (*): $P < 0.05$; double asterisks (**): $P < 0.01$. Data are presented as mean ± S.E.M.

Discussion

Engineered nanomaterials hold significant potential for enhancing disease diagnosis and treatment specificity. By employing cell-specific targeting, molecular transport to particular organelles, and other strategies, nanotechnology can overcome traditional delivery limitations such as biodistribution issues and intracellular transport barriers. Nanomaterials can also increase the stability and solubility of encapsulated drugs, promote transmembrane transport, and extend circulatory half-lives, ultimately improving the safety and efficacy of drug applications.[27,28] Consequently, nanomedicine research has been widely used, yielding promising results *in vitro* and in animal model experiments.[29] Compared with inorganic NPs, organic polymeric NPs have good advantages in terms of biocompatibility and biodegradation, and can be prepared into liposomes, polymer micelles, polymer hydrogels, polymer couplings, and other forms of drug nanocarriers. If gene therapy, especially the silencing effect of siRNA on target genes, is combined with the application of nanomaterials, it

may also have good prospects for the long-term treatment of autoimmune diseases.[30,31]

Biodegradable polymer particles provide a versatile platform for immune system signaling, as they can be easily surface-modified to target specific receptors and are designed to release encapsulated drugs in a controlled, sustained manner.[32,33] To address the challenge of low encapsulation efficiency of hydrophobic drugs in traditional methods, Bershteyn *et al.* wrapped polyethylene glycol phospholipid (PEG) bilayers on PLGA particles to synthesize nanospheres that self-assemble, forming nanospheres with a hydrophilic core and hydrophobic coating suitable for both hydrophilic and hydrophobic cargoes.[34] In this study, a cationic lipid-assisted PEG-PLGA nanoparticle was investigated for efficient co-delivery of a hydrophobic small molecule drug (VD3) and a hydrophilic nucleic acid drug (siLkb1) *in vivo*. The particles simultaneously encapsulated hydrophobic (VD3) and hydrophilic (siRNA) drugs, maintaining nanoscale dimensions and a stable positive surface charge. Due to the encapsulation of negatively charged siRNA and larger particle size, the mass of polymer nanomaterials and the adsorption of cationic liposomes within NPs/VD3/siLkb1 increased, thus increasing the encapsulation efficiency of VD3. Nanoparticles within 20 to 200 nm were reported to be more readily diverted to the lymph nodes and endocytosed early by APC residents in the lymph nodes, thus presenting the antigen.[35] The particle size that we produced was within this range. The method of administration was intradermal injection in the draining lymph node area. Subsequently, the nanoparticles' effective phagocytosis by DCs and drug delivery into cells were confirmed both *in vitro* and *in vivo*. We expect to regulate the phenotypic changes of dendritic cells using this particle while expanding the Treg cell pool to achieve immunomodulation.

As immune sentinels, dendritic cells play a crucial role in regulating immune responses. They absorb and process antigens on the MHC, present the antigens to T cells, and then activate T cells through the expression of costimulatory factors CD40 and CD80/CD86 acting on T cells surface ligands, resulting in an immune response.[6,36] DCs can induce either an inflammatory or tolerogenic response, depending on cell subtypes and stimuli received from their local environment. This dual capability of DCs enhances the therapeutic interest in altering immune activation by generating TolDC. Characterized by lower expression levels of MHC-II and co-stimulatory molecules than normal DCs, TolDC is a stable, semi-mature dendritic cell subset that produces low levels of pro-inflammatory cytokines and high levels of immunomodulatory cytokines.[37] TolDC-induced immune tolerance mechanisms include (1) T cell depletion; (2) T cell inactivation induction; (3) T cell cytokine profile deviations (*e.g.*, from T helper type 1 (Th1) to T helper type 2 (Th2)); and (4) Treg induction. Additionally, TolDC may directly inhibit immune responses through the secretion of immunosuppressive molecules.[38,39] In contrast to immature DCs, TolDC remains in a stable, semi-mature state even when encountering infectious agents, while immature DCs become mature DCs.[40]

VD3, one of several compounds capable of inducing the change of DCs to the TolDC subtype, not only acts on the vitamin D receptor (VDR) on the surface of lymphocytes[8] for immune regulation, but also reduces the expression of surface molecules on DCs, thereby inducing the TolDC phenotype and treating transplant rejection[41] and autoimmune diseases such as non-obese diabetes (NOD) and rheumatoid arthritis.[42,43] We obtained similar results with VD3-loaded polymer nanoparticles reported previously, wherein NPs/VD3 could downregulate the expression of CD86, CD40, and MHC-II on DCs *in vitro* and *in vivo*, successfully inducing and maintaining the phenotype of TolDC.[44,45] However, the *in vivo* amplification of Treg levels remains limited.

Treg cells, a subset of $CD4^+$ T cells, maintain immune tolerance[46] and play a critical role in controlling autoimmunity; thus, strategies to enhance their activity and number may imply a therapeutic avenue for autoimmune diseases.[47] To further expand the Treg pool, we co-regulated Lkb1 expression in DCs while administering VD3. Lkb1, a serine/threonine kinase, activates AMPK at low intracellular ATP levels, inducing catabolism and oxidative metabolism.[48] Treg cells utilize Lkb1 signaling to coordinate their metabolism and immune homeostasis, controlling the balance between immunity and tolerance, while the loss of Lkb1 impairs Treg survival and function.[49,50] Recently, Lkb1 was found to play a role in DCs' regulation of Treg cell differentiation. The loss of Lkb1 also results in aberrant DC maturation and the production of cytokines and immunomodulatory molecules.[15] Lkb1-deficient DCs upregulate OX40L expression by inhibiting the NF-κB pathway, thereby expanding Treg cells,[51] and promoting the proliferation of functional Treg cells by enhancing mTOR signaling through the AMPK signaling pathway.[15,16] In this study, Lkb1-siRNA-encapsulated PEG-PLGA NPs downregulated the expression of Lkb1 in DCs. Although NPs/siLkb1 did not effectively alter the expression of molecules on the surface of DC cells *in vitro* and *in vivo*, it still amplified the Treg cell pool compared to NPs/siNC. Some scholars have shown that knockout of the Lkb1 gene in DCs can promote the increase of thymus-derived Treg production and peripheral output.[51] In this study, target gene silencing after siRNA administration was weaker than gene knockouts. Nevertheless, the co-delivery of VD3 and siLkb1 by PEG-PLGA not only induced and maintained the TolDC phenotype *in vitro* and *in vivo* but also significantly expanded the ratio and count of Treg cells *in vivo*. In the treatment experiment using EAE as an animal model, all nanoparticle treatment groups induced immune tolerance, considering the properties of the PEG-PLGA material itself. Some studies have shown that PLGA carriers, after phagocytosis by APC cells, produce the metabolic intermediate lactic acid, which has anti-inflammatory capacity,[52] allowing NPs/siNC to have some effect in treating EAE. However, the therapeutic effect and histological evaluation of NPs/VD3/siLkb1 were significantly better than those of the other groups. These data suggest that VD3 and Lkb1-siRNA delivered to peripheral lymphoid organ-draining lymph nodes may act synergistically to differentiate DCs towards the TolDC phenotype while expanding Tregs. However, its underlying mechanism requires further exploration.

Conclusion

In summary, we have successfully developed a PEG-PLGA drug delivery system capable of simultaneously encapsulating VD3 and Lkb1-siRNA for combined application in DC cells. Upon intradermal injection in the inguinal region, the payload rapidly accumulated and was released in the draining lymph nodes. Subsequent to phagocytosis by DC cells, NPs/VD3/siLkb1 induced and maintained phenotypic changes in TolDC by reducing the expression of dendritic cell surface molecules, while simultaneously amplifying Treg levels. Notably, in the treatment of mice with EAE as a model of autoimmune disease, the onset time was significantly delayed and the disease severity diminished. This study offers a reliable therapeutic approach for the treatment of autoimmune diseases; however, the underlying mechanism warrants further detailed exploration.

Author contributions

H.-C.L. designed, performed, and analyzed data from most of the studies. He also helped write the manuscript with input from all authors. H.L., J.W., and X.C. helped in the performance of flow cytometry studies. Y.X. helped in the nanoparticle experiment. X.G. conceived and designed the animal studies. Q.-S.Z. contributed to the literature search. T.S., B.C., Y.Z., and Y.-G.Y. conceived, designed, and supervised all studies, and participated in the drafting and editing of the manuscript. All authors contributed to the critical review of the manuscript.

Conflicts of interest

The authors declare that the research was conducted in the absence of any commercial or financial relationships that could be construed as a potential conflict of interest.

Acknowledgements

This work was supported by grants from the NSFC (82000120, 32171379, 81941008), the China Postdoctoral Science Foundation (2020M681049), the Interdisciplinary Innovation Project of the First Hospital of Jilin University (JDYYJCHX001), and the Fundamental Research Funds for the Central Universities, JLU.

References

1 T. M. Rivers and F. F. Schwentker, Encephalomyelitis Accompanied by Myelin Destruction Experimentally Produced in Monkeys, *J. Exp. Med.*, 1935, **61**(5), 689–702.
2 T. Worbs, S. I. Hammerschmidt and R. Forster, Dendritic cell migration in health and disease, *Nat. Rev. Immunol.*, 2017, **17**(1), 30–48.
3 J. Hu and Y. Wan, Tolerogenic dendritic cells and their potential applications, *Immunology*, 2011, **132**(3), 307–314.
4 S. Yoo and S. J. Ha, Generation of Tolerogenic Dendritic Cells and Their Therapeutic Applications, *Immune Netw.*, 2016, **16**(1), 52–60.
5 V. Mastorodemos, M. Ioannou and P. Verginis, Cell-based modulation of autoimmune responses in multiple sclerosis and experimental autoimmmune encephalomyelitis: therapeutic implications, *Neuroimmunomodulation*, 2015, **22**(3), 181–195.
6 A. Compston and A. Coles, Multiple sclerosis, *Lancet*, 2008, **372**(9648), 1502–1517.
7 L. Legroux and N. Arbour, Multiple Sclerosis and T Lymphocytes: An Entangled Story, *J. Neuroimmune Pharmacol.*, 2015, **10**(4), 528–546.
8 M. A. Maestro, F. Molnar, A. Mourino and C. Carlberg, Vitamin D receptor 2016: novel ligands and structural insights, *Expert Opin. Ther. Pat.*, 2016, **26**(11), 1291–1306.
9 C. E. Hayes, S. L. Hubler, J. R. Moore, L. E. Barta, C. E. Praska and F. E. Nashold, Vitamin D Actions on CD4 (+) T Cells in Autoimmune Disease, *Front. Immunol.*, 2015, **6**, 100.
10 A. H. Muris, J. Smolders, L. Rolf, M. Thewissen, R. Hupperts, J. Damoiseaux, *et al.*, Immune regulatory effects of high dose vitamin D3 supplementation in a randomized controlled trial in relapsing remitting multiple sclerosis patients receiving IFNbeta; the SOLARIUM study, *J. Neuroimmunol.*, 2016, **300**, 47–56.
11 F. Ashtari, N. Toghianifar, S. H. Zarkesh-Esfahani and M. Mansourian, Short-term effect of high-dose vitamin D on the level of interleukin 10 in patients with multiple sclerosis: a randomized, double-blind, placebo-controlled clinical trial, *Neuroimmunomodulation*, 2015, **22**(6), 400–404.
12 D. S. da Costa, J. Hygino, T. B. Ferreira, T. M. Kasahara, P. O. Barros, C. Monteiro, *et al.*, Vitamin D modulates different IL-17-secreting T cell subsets in multiple sclerosis patients, *J. Neuroimmunol.*, 2016, **299**, 8–18.
13 E. S. Sotirchos, P. Bhargava, C. Eckstein, K. Van Haren, M. Baynes, A. Ntranos, *et al.*, Safety and immunologic effects of high- vs low-dose cholecalciferol in multiple sclerosis, *Neurology*, 2016, **86**(4), 382–390.
14 J. C. Gallagher, Vitamin D and falls - the dosage conundrum, *Nat. Rev. Endocrinol.*, 2016, **12**(11), 680–684.
15 Y. Wang, X. Du, J. Wei, L. Long, H. Tan, C. Guy, *et al.*, LKB1 orchestrates dendritic cell metabolic quiescence and antitumor immunity, *Cell Res.*, 2019, **29**(5), 391–405.
16 L. R. Pelgrom, T. A. Patente, A. Sergushichev, E. Esaulova, F. Otto, A. Ozir-Fazalalikhan, *et al.*, LKB1 expressed in dendritic cells governs the development and expansion of thymus-derived regulatory T cells, *Cell Res.*, 2019, **29**(5), 406–419.
17 A. Babu, R. Muralidharan, N. Amreddy, M. Mehta, A. Munshi and R. Ramesh, Nanoparticles for siRNA-Based Gene Silencing in Tumor Therapy, *IEEE Trans Nanobiosci.*, 2016, **15**(8), 849–863.

18 Y. Deng, C. C. Wang, K. W. Choy, Q. Du, J. Chen, Q. Wang, *et al.*, Therapeutic potentials of gene silencing by RNA interference: principles, challenges, and new strategies, *Gene*, 2014, **538**(2), 217–227.
19 K. A. Whitehead, R. Langer and D. G. Anderson, Knocking down barriers: advances in siRNA delivery, *Nat. Rev. Drug Discovery*, 2009, **8**(2), 129–138.
20 J. E. Zuckerman and M. E. Davis, Clinical experiences with systemically administered siRNA-based therapeutics in cancer, *Nat. Rev. Drug Discovery*, 2015, **14**(12), 843–856.
21 J. W. Hickey, J. L. Santos, J. M. Williford and H. Q. Mao, Control of polymeric nanoparticle size to improve therapeutic delivery, *J. Controlled Release*, 2015, **219**, 536–547.
22 M. Afsharzadeh, M. Hashemi, A. Mokhtarzadeh, K. Abnous and M. Ramezani, Recent advances in co-delivery systems based on polymeric nanoparticle for cancer treatment, *Artif. Cells, Nanomed., Biotechnol.*, 2018, **46**(6), 1095–1110.
23 M. Caldorera-Moore, J. E. Vela Ramirez and N. A. Peppas, Transport and delivery of interferon-alpha through epithelial tight junctions via pH-responsive poly(methacrylic acid-grafted-ethylene glycol) nanoparticles, *J. Drug Targeting*, 2019, **27**(5–6), 582–589.
24 F. C. Knight, P. Gilchuk, A. Kumar, K. W. Becker, S. Sevimli, M. E. Jacobson, *et al.*, Mucosal Immunization with a pH-Responsive Nanoparticle Vaccine Induces Protective CD8(+) Lung-Resident Memory T Cells, *ACS Nano*, 2019, **13**(10), 10939–10960.
25 L. Zhang, A. Beatty, L. Lu, A. Abdalrahman, T. M. Makris, G. Wang, *et al.*, Microfluidic-assisted polymer-protein assembly to fabricate homogeneous functionalnanoparticles, *Mater. Sci. Eng., C*, 2020, **111**, 110768.
26 J. L. Urban, V. Kumar, D. H. Kono, C. Gomez, S. J. Horvath, J. Clayton, *et al.*, Restricted use of T cell receptor V genes in murine autoimmune encephalomyelitis raises possibilities for antibody therapy, *Cell*, 1988, **54**(4), 577–592.
27 L. Kou, Y. D. Bhutia, Q. Yao, Z. He, J. Sun and V. Ganapathy, Transporter-Guided Delivery of Nanoparticles to Improve Drug Permeation across Cellular Barriers and Drug Exposure to Selective Cell Types, *Front. Pharmacol.*, 2018, **9**, 27.
28 E. Blanco, H. Shen and M. Ferrari, Principles of nanoparticle design for overcoming biological barriers to drug delivery, *Nat. Biotechnol.*, 2015, **33**(9), 941–951.
29 S. Mitragotri, T. Lammers, Y. H. Bae, S. Schwendeman, S. De Smedt, J. C. Leroux, *et al.*, Drug Delivery Research for the Future: Expanding the Nano Horizons and Beyond, *J. Controlled Release*, 2017, **246**, 183–184.
30 M. Zhao, R. Wang, K. Yang, Y. Jiang, Y. Peng, Y. Li, *et al.*, Nucleic acid nanoassembly-enhanced RNA therapeutics and diagnosis, *Acta Pharm. Sin. B*, 2023, **13**(3), 916–941.
31 T. Su, X. Feng, J. Yang, W. Xu, T. Liu, M. Zhang, *et al.*, Polymer nanotherapeutics to correct autoimmunity, *J. Controlled Release*, 2022, **343**, 152–174.
32 T. G. Park, Degradation of poly(lactic-co-glycolic acid) microspheres: effect of copolymer composition, *Biomaterials*, 1995, **16**(15), 1123–1130.
33 M. S. Shive and J. M. Anderson, Biodegradation and biocompatibility of PLA and PLGA microspheres, *Adv. Drug Delivery Rev.*, 1997, **28**(1), 5–24.
34 A. Bershteyn, M. C. Hanson, M. P. Crespo, J. J. Moon, A. V. Li, H. Suh, *et al.*, Robust IgG responses to nanograms of antigen using a biomimetic lipid-coated particle vaccine, *J. Controlled Release*, 2012, **157**(3), 354–365.
35 Q. Wei, Y. Su, H. Xin, L. Zhang, J. Ding and X. Chen, Immunologically Effective Biomaterials, *ACS Appl. Mater. Interfaces*, 2021, **13**(48), 56719–56724.
36 L. Fugger, L. T. Jensen and J. Rossjohn, Challenges, Progress, and Prospects of Developing Therapies to Treat Autoimmune Diseases, *Cell*, 2020, **181**(1), 63–80.
37 H. Li and B. Shi, Tolerogenic dendritic cells and their applications in transplantation, *Cell. Mol. Immunol.*, 2015, **12**(1), 24–30.
38 R. M. Steinman, D. Hawiger and M. C. Nussenzweig, Tolerogenic dendritic cells, *Annu. Rev. Immunol.*, 2003, **21**, 685–711.
39 O. Morante-Palacios, F. Fondelli, E. Ballestar and E. M. Martinez-Caceres, Tolerogenic Dendritic Cells in Autoimmunity and Inflammatory Diseases, *Trends Immunol.*, 2021, **42**(1), 59–75.
40 M. B. Lutz, Therapeutic potential of semi-mature dendritic cells for tolerance induction, *Front. Immunol.*, 2012, **3**, 123.
41 G. B. Ferreira, E. van Etten, A. Verstuyf, M. Waer, L. Overbergh, C. Gysemans, *et al.*, 1,25-Dihydroxyvitamin D3 alters murine dendritic cell behaviour in vitro and in vivo, *Diabetes/Metab. Res. Rev.*, 2011, **27**(8), 933–941.
42 E. van Etten, O. Dardenne, C. Gysemans, L. Overbergh and C. Mathieu, 1,25-Dihydroxyvitamin D3 alters the profile of bone marrow-derived dendritic cells of NOD mice, *Ann. N. Y. Acad. Sci.*, 2004, **1037**, 186–192.
43 F. M. J. Hafkamp, T. G. Kormelink and E. C. de Jong, Targeting DCs for Tolerance Induction: Don't Lose Sight of the Neutrophils, *Front. Immunol.*, 2021, **12**, 732992.
44 M. Bscheider and E. C. Butcher, Vitamin D immunoregulation through dendritic cells, *Immunology*, 2016, **148**(3), 227–236.
45 R. A. Harry, A. E. Anderson, J. D. Isaacs and C. M. Hilkens, Generation and characterisation of therapeutic tolerogenic dendritic cells for rheumatoid arthritis, *Ann. Rheum. Dis.*, 2010, **69**(11), 2042–2050.
46 M. Buc, Role of regulatory T cells in pathogenesis and biological therapy of multiple sclerosis, *Mediators Inflammation*, 2013, **2013**, 963748.
47 L. Goschl, C. Scheinecker and M. Bonelli, Treg cells in autoimmunity: from identification to Treg-based therapies, *Semin. Immunopathol.*, 2019, **41**(3), 301–314.
48 S. K. Wculek and D. Sancho, LKB1 restrains dendritic cell function, *Cell Res.*, 2019, **29**(6), 429–431.
49 K. Yang, D. B. Blanco, G. Neale, P. Vogel, J. Avila, C. B. Clish, *et al.*, Homeostatic control of metabolic and functional fitness of Treg cells by LKB1 signalling, *Nature*, 2017, **548**(7669), 602–606.
50 D. Wu, Y. Luo, W. Guo, Q. Niu, T. Xue, F. Yang, *et al.*, Lkb1 maintains Treg cell lineage identity, *Nat. Commun.*, 2017, **8**, 15876.

51 S. Chen, L. Fang, W. Guo, Y. Zhou, G. Yu, W. Li, *et al.*, Control of Treg cell homeostasis and immune equilibrium by Lkb1 in dendritic cells, *Nat. Commun.*, 2018, **9**(1), 5298.

52 R. P. Allen, A. Bolandparvaz, J. A. Ma, V. A. Manickam and J. S. Lewis, Latent, Immunosuppressive Nature of Poly (lactic-co-glycolic acid) Microparticles, *ACS Biomater. Sci. Eng.*, 2018, **4**(3), 900–918.